Molecular Modeling of the Axial and Circumferential Elastic Moduli of Tubulin

A. S. Zeiger*† and B. E. Layton†

*Materials Science Department, Massachusetts Institute of Technology, Cambridge, Massachusetts; and †Drexel University, Department of Mechanical Engineering and Mechanics, Philadelphia, Pennsylvania

ABSTRACT Microtubules play a number of important mechanical roles in almost all cell types in nearly all major phylogenetic trees. We have used a molecular mechanics approach to perform tensile tests on individual tubulin monomers and determined values for the axial and circumferential moduli for all currently known complete sequences. The axial elastic moduli, in vacuo, were found to be 1.25 GPa and 1.34 GPa for α- and β-bovine tubulin monomers. In the circumferential direction, these moduli were 378 MPa for α- and 460 MPa for β-structures. Using bovine tubulin as a template, 269 homologous tubulin structures were also subjected to simulated tensile loads yielding an average axial elastic modulus of 1.10 ± 0.14 GPa for α-tubulin structures and 1.39 ± 0.68 GPa for β-tubulin. Circumferentially the α- and β-moduli were 936 ± 216 MPa and 658 ± 134 MPa, respectively. Our primary finding is that that the axial elastic modulus of tubulin diminishes as the length of the monomer increases. However, in the circumferential direction, no correlation exists. These predicted anisotropies and scale dependencies may assist in interpreting the macroscale behavior of microtubules during mitosis or cell growth. Additionally, an intergenomic approach to investigating the mechanical properties of proteins may provide a way to elucidate the evolutionary mechanical constraints imposed by nature upon individual subcellular components.

INTRODUCTION

Microtubules provide a number of mechanical services in nearly all cell types throughout most of the major branches of the phylogenetic tree including archaea (1). They act as mitotic spindles for cell division (2), maintain transport conduits (3,4), and are used as flagella (5). Recently, they have also been implicated as playing a critical role in consciousness (6). Additionally, microtubules interact with actin filaments and the cellular membrane to provide a foundation that determines cell morphology (7,8). While typically constructed of a heterodimeric lattice, with intermonomeric bond stiffnesses and strengths contributing to cellular-scale behavior, microtubule function and assembly may also be attributed to the mechanical properties of individual tubulin monomers. While tubulin sequences vary significantly across species, the role that specific residues or tertiary-scale interactions contribute to the ultimate behavior of tubulin is difficult to predict (e.g., (9)).

Experimental approaches to determine the mechanical properties of tubulin have included optical tweezers (8), hydrodynamic flow (10), vesicle buckling (11), thermally induced vibrations (12), naturally occurring bending (13), and atomic force microscopy (14). Most of these experiments focus on obtaining buckling stiffness of microtubules and have yielded a wide range of values for axial elastic modulus, 1 MPa to 7 GPa (1 MPa = 1 megapascal = 10^6 N/m^2; 1 GPa = 1 gigapascal = 10^9 N/m^2). These findings have been well reviewed (15).

Modeling approaches for predicting tubulin and microtubule properties include those of Tuszynski et al. (16) and Kerssemakers et al. (17). Often, simulations are run in vacuo, which reduces computational requirements by an exponential factor versus models employing implicit or explicit water. One of the first exhaustive three-dimensional intergenomic homology modeling studies of tubulin focused mainly on geometry, dipole moments, charge distributions, and C-terminus lattice structures, was by Tuszynski et al. (18). Their results offer an exhaustive comparison for the structural properties of homologous tubulin structures in Tuszynski et al. (19), but did not explore mechanical properties.

Here, we establish a framework comparing mechanical properties of members of the same family of proteins. We have performed molecular mechanics simulations on all of the currently sequenced α-, β-, and γ-tubulins. Specifically, we simulated axial and circumferential loading on all structures after mapping them onto a consensus structure (20). Our findings may elucidate the roles that key mutations or conserved regions may have played in driving tubulin toward its mechanically anisotropic state. Additionally, the mechanical effects of directed mutations, or of engineered protein sequences, may be estimated before employing molecular biological techniques.

For special terms and reference data used in this article, see Table 1.

Submitted February 21, 2008, and accepted for publication June 19, 2008.

Address reprint requests to Bradley Edward Layton, Tel.: 215-895-1752; E-mail: blay@drexel.edu; or E-mail: blay@alum.mit.edu.

Editor: Kathleen B. Hall.

0006-3495/08/10/3606/13 $2.00

doi: 10.1529/biophysj.108.131359

TABLE 1 Notation

D_i	Inner diameter of tubulin
D_0	Outer diameter of tubulin
E_{MT}	Elastic modulus of tubulin
E_{mono}	Elastic modulus of monomer
E	Elastic (Young's) modulus
F_i	Force on a MT filament
I	Second moment of inertia
K^*	Inverse stiffness of dimer
k_α	Stiffness of α-tubulin
k_β	Stiffness of β-tubulin
$k_{\alpha\beta}$	Stiffness of monomer-monomer bond
$k_{\beta\alpha}$	Stiffness of dimer-dimer bond
k_B	Boltzmann's constant, 1.38×10^{-23} J/K
k_i^{bond}	Axial stiffness of covalent bond
k_i^{angle}	Rotational stiffness of covalent bond
$k_i^{dihedral}$	Torsional stiffness of covalent bond
L_0	Unstrained dimer length
l_p	Persistence length
L_z	Axial length of monomer
ΔL	Change in length
M_r	Bending moment
n_i	Crystal plane number
r	Radial direction
r_i	Stretched bond length
r_{ij}	Atomic separation for Coulomb force
r_{oi}	Equilibrium bond length
T	Temperature
U_{total}	Total simulation energy
U_{bond}	Energy from bond stretching
U_{angle}	Energy from bond bending
$U_{dihedral}$	Energy from bond twisting
U_{vdW}	Energy from van der Waals interactions
$U_{Coulomb}$	Energy from Coulomb interactions
z	Axial direction
γ_i	Equilibrium value of ϕ
Δ_α	Deformation of α-tubulin
Δ_β	Deformation of β-tubulin
$\Delta_{\alpha\beta}$	Deformation of monomer-monomer bond
$\Delta_{\beta\alpha}$	Deformation of dimer-dimer bond
ε	Strain
ε_{ij}	Maximum energy of separation
ε_0	Permittivity of free space
θ	Circumferential direction
θ_i	Circumferential position of filament in MT
θ_I	bent bond angle
θ_{oi}	Equilibrium bond angle
κ	Curvature
O_i	Tetrahedral bond angle
ρ	Radius of curvature
σ_{ij}	Zero energy separation distance
ϕ_i	Angle between bond planes

METHODS

Sequences used

We searched for all complete primary tubulin sequences within the Research Collaboratory for Structural Bioinformatics Protein Data Bank (PDB) (21). Utilizing the UniProt protein resource (22), we were able to obtain sequences for 269 tubulin structures. This series includes 96 α-structures, 147 β-structures, and 26 γ-structures. To date, a few hundred tubulin sequences have been identified and sequenced. Even fewer (only two or three) three-dimensional structures of tubulin dimers exist at a significantly high resolution to produce accurate homology models (21).

Structural homology matching

Since the tertiary structures of all nearly all of the presently sequenced tubulins are unknown, a three-dimensional consensus structure template was needed. For this, we selected the highest-resolution structure produced to date. Lowe et al. obtained a 3.5 Å resolution structure of the α-β dimer for bovine tubulin utilizing electron diffraction (PDB Identifier 1JFF) (20). This predicted structure corresponds to that of the tubulin dimer found in zinc-induced tubulin sheets. Although there has been no systematic study to compare the sheet structure with the cylindrical structure, it is reasonable to assume that the individual dimers and monomers within the sheet are more flat in the circumferential direction. Recent simulation and imaging work (24) of a 15-filament structure indicates that the GDP-versus-GTP state of β-tubulin may be responsible for microtubule stability. Specifically, Krebs et al. (24) suggest that, since the 15-filament structure represents an intermediate form between the ~10-nm radius-of-curvature of a native microtubule and the infinite radius-of-curvature of the zinc-induced sheets, it may serve as a predictor of microtubule stability. Ideally, for microtubule-scale mechanical property prediction, tubulin-straining simulations such as those we have performed would be done on the curved configuration. However, since current experimental techniques preclude this level of detail, we are limited to the sheet configuration.

For γ-tubulin, we used the 2.71 Å resolution structure (PDB Identifier 1Z5V) obtained by Aldaz et al. (25). Utilizing the structure predicted by Lowe et al. (20) as a template for other α-β-tubulin structures, and Aldaz's structure for γ-tubulin, we created homology models of all tertiary structures. We began by using nanoscale molecular dynamics (NAMD) downloaded from the University of Illinois at Urbana-Champagne's Theoretical and Computational Biophysics Group (26) and separated the dimers into their monomeric units. From the dimer PDB files, a protein structure file (PSF) was created using NAMD's psfgen package, the topology file required for this PSF (using Chemistry at Harvard Molecular Mechanics, i.e., CHARMM, Ver. 22, for proteins and lipids). Topology files contain bond connectivity, angle, and charge distribution information. The parameter file, also CHARMM Ver. 22, contains force constants, equilibrium geometries, and various other calculations required to perform energy balances (27,28). Cutoffs were set in the force-field parameters at 12 Å. At 20 steps per cycle, and a 100-step minimization was performed on the monomer to produce a local minimum energy structure for α-, β-, and γ-tubulin (Fig. 1). This approach was necessary because the problem of de novo prediction of three-dimensional structure from a one-dimensional sequence is exceedingly difficult and frequently yields nonunique solutions (29).

To perform energy minimization of the structures to be stretched we used SWISS-MODEL (http://swissmodel.expasy.org/SWISS-MODEL.html). Briefly, SWISS-MODEL follows the following protocol: initially it checks the sequence identity with the target. It then creates a ProModII job by first superimposing three-dimensional structures of the two related proteins and generates multiple alignments with the sequence to be modeled. By using the positions of atoms that are most similar between the template structure and predicted structure, it creates a framework and rebuilds any lacking loops. It then completes and corrects the backbone structure and the side chains, verifies the model structure quality, and finally refines the structure with energy minimization using GROMOS96. Lastly, a PDB file is produced and BLAST analysis is provided. The series of amino-acid sequences produced an average similarity of 85.82% and standard deviation of 9.39% with the template structures. Structures with a similarity at $<25\%$ were automatically rejected by the SWISS-MODEL server. Sequences with $<50\%$ similarity were usually a result of incomplete or fragmentary structures. However, these structures were still included in the simulation of stretching the tubulin structures. Sequence alignment and similarities were independently verified using CLUSTAL W (30).

To enhance the likelihood of finding the likely global minimal energy structure, in several test cases, we allowed our minimization procedure to run for 10,000 steps rather than the recommended 100 steps of steepest descent, followed by 200–300 steps of conjugate gradient energy minimization. In these extended simulations, no more than 5–10% difference was observed in total energy. Only one structure failed to stabilize (TBA8_CAEEL), regard-

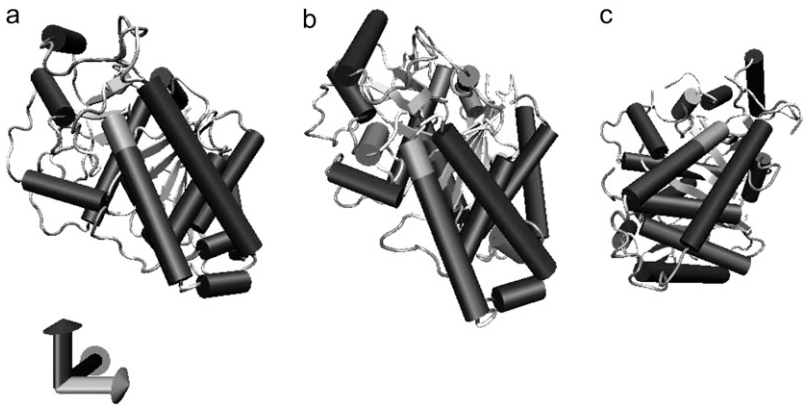

FIGURE 1 Template structures: (*a*) 1JFFA bovine α-tubulin (20), (*b*) 1JFFB bovine β-tubulin (20), (*c*) 1Z5VG human γ-tubulin (25) VMD atomic structures (67). The view is from the inside. The vertical arrow points toward the ''plus'' end, or growing end. In neurons, this end is furthest from the nucleus.

less of the number of time steps (31). While the sequences of all tubulin structures we studied are published, their exact three-dimensional structures have yet to be determined. Once the 269 tubulin homologous models were created, visual molecular dynamics (VMD) was used to visualize the structures to verify that three-dimensional consensus mapping resulted in globular protein structures of densities comparable to the template structure. All structural predictions were performed in vacuo. While this is a limitation of the model, since the force constants developed for NAMD through CHARMM were developed within an explicit water framework, recent work using a ubiquitin model indicates that this approach leads to errors that are statistically insignificant ($p < 0.01$) (32).

The majority of the structural data for MT(microtubule)s has been acquired from highly purified preparations, thus our simulations most likely closely represent the material behavior of tubulin in isolated microtubules. In a manner consistent with Tuszynski's approach, we worked under the assumption that errors within each model are negligible when compared against a group of models (19). This error can be reduced by using an initial minimization run before the tensile test is performed. Another notable quality of the molecular deformation experiments is that in general, the α-tubulin molecules exhibit multiple moduli as the protein unfolds (see Fig. 5). This type of behavior has been observed in fabric failure (34), but is not observed in solid structures.

Parameters used, boundary conditions, and optimization

Steered molecular dynamics (SMD) offers programmable dynamic simulation utilizing NAMD (35). The NAMD software was loaded with the original PDB files, PSF file, a reference file (1JFF and 1Z5V), and a configuration file to perform the simulation following previously developed methods (21,36). Briefly, NAMD is a parallel molecular dynamics code specifically designed for the simulation of large biomolecular systems. The software is open-source and available free of charge. It allows the user to perform chemical and conformation free energy calculations with multiple timestep integration. For our application, the ability to create scriptable code in Tool Command Language integrated with SMD allowed us to perform repeatable dynamic simulations of all structures we considered with the exception of one incomplete sequence: TBA8_CAEEL.

While there are no standards for simulated molecular mechanical property characterization, standard macroscale mechanical tensile tests utilize dog-bone-shaped specimens to ensure a concentration of loading on a narrow portion of the sample with a precisely known cross-sectional area. In general, these tests result in a scale-invariant elastic modulus until smaller dimensions are reached, where moduli tend to increase and become more variable (37,38). While single molecule experiments have been performed on single proteins as they unfold (e.g., (39)), the opportunity to interrogate a single tubulin monomer in its naturally occurring state has not been realized. Thus, the Cartesian coordinates for every atom in the PDB structure were tabulated to determine a suitable region to act as a grasping area. This is shown in Fig. 2, which depicts a histogram of the distribution for a human tubulin species, similar to that of 1JFFB, in the axial direction. A histogram of the *z*-axis positions of each atom as provided in the PDB files was plotted in 3.3 Å increments using MS Excel. The C-termini tails of tubulin monomers, because of the extensive number of possible interactions that are still undetermined, were cut off before performing the simulations. Thus, an entire line of residues was removed—preventing the possibility that this relatively flexible region would dictate the simulation behavior. To facilitate our virtual tensile testing, we labeled 10% of the most distal N-terminus atoms as fixed atoms and 20% of the remaining most distal C-terminus atoms as steered atoms. These atoms were labeled appropriately in each PDB file with a value of 1.00 in the appropriate Fixed or Steered column.

We used SMD to pull the 6377-atom α-monomer and 6574-atom β-monomer in tension. Fixed atoms were held rigid, while steered atoms were directed by an SMD atom, pulled axially at 0.005 Å per time step. This translates to 2.5 Å/ps with a time step of 2 fs. The SMD ''dummy'' atom pulls the steered atom with a spring constant of 7 kcal mol^{-1} Å^{-2} $\cong$ 500 pN Å^{-1} = 5 Nm^{-1}, (1 kcal/mol^{-1} = 69.5 pN Å).

These values were selected based upon a series of optimization simulations. We performed an initial set of simulations on the 1JFF β-monomer at a series of velocities ranging from 0.5 to 0.005 Å/ns. A velocity of 0.05 Å/ns was found to be asymptotic in that it achieved an elastic modulus that was within 2% of the modulus measured at the slower velocities. At velocities slower than this, computational time became unreasonable and produced errors in energy minimization cascades over long time-periods. Simulations run faster than 0.05 Å/ns resulted in inaccuracies caused by overstretched bond angles (Fig. 3). The velocity of pulling also reflects the effect of hy-

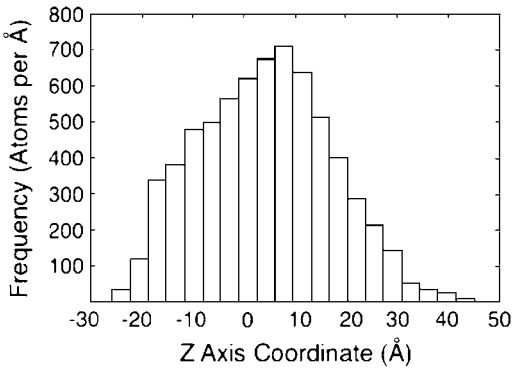

FIGURE 2 Histogram of atom distribution in TBA1_HUMAN ((68–72); W. V. Bienvenut, and D. Claeys, unpublished). The N-terminus of the protein is located at −20 Å. Most of the tubulin structures have relatively long C-terminus tails. *Z* is parallel to microtubule major axis.

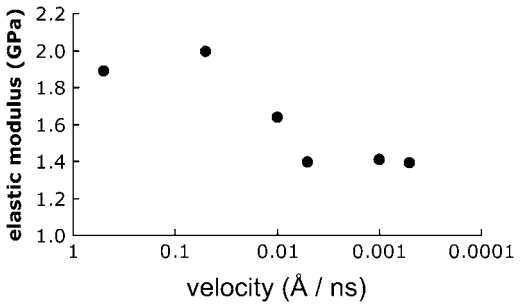

FIGURE 3 To optimize computational resources, we performed our simulations at a series of velocities ranging from 0.5 to 0.005 Å/ns. At rates <0.05 Å/ns, modulus results were unaffected.

drogen embrittlement on the atomic structure. In calculating the iterative energies, the presence of hydrogen adds an extra force component to the system. In reality, the monomer may be more plastic as a consequence of hydrating the structure, resulting in lower moduli. Faster pulling rates also result in more brittle behavior (40).

Total simulation energy, U_{total}, is calculated as a sum of contributions from three primary deformation modes (35,42), as well as van der Waals forces and Coulomb forces, as

$$U_{\text{total}} = U_{\text{bond}} + U_{\text{angle}} + U_{\text{dihedral}} + U_{\text{vdW}} + U_{\text{Coulomb}}. \quad (1)$$

Each of these individual energies are found from

$$U_{\text{bond}} = \sum_{\text{bonds i}} k_{\text{i}}^{\text{bond}}(r_{\text{i}} - r_{\text{oi}})^2,$$

$$U_{\text{angle}} = \sum_{\text{angles i}} k_{\text{i}}^{\text{angle}}(\theta_{\text{i}} - \theta_{\text{oi}})^2,$$

$$U_{\text{dihedral}} = \sum_{\text{dihedral i}} \begin{cases} k_{\text{i}}^{\text{dihedral}}[1 + \cos(n_{\text{i}}\phi_{\text{i}} - \gamma_{\text{i}})], & n_{\text{i}} \neq 0 \\ k_{\text{i}}^{\text{dihedral}}(\text{O}_{\text{i}} - \gamma_{\text{i}})^2, & n_{\text{i}} = 0 \end{cases},$$

$$U_{\text{vdW}} = \sum_{\text{i}}\sum_{\text{j>i}} 4\varepsilon_{\text{ij}}\left[\left(\frac{\sigma_{\text{ij}}}{r_{\text{ij}}}\right)^{12} - \left(\frac{\sigma_{\text{ij}}}{r_{\text{ij}}}\right)^{6}\right], \text{ and}$$

$$U_{\text{Coulomb}} = \sum_{\text{i}}\sum_{\text{j>i}} \frac{q_{\text{i}}q_{\text{j}}}{4\pi\varepsilon_{\text{o}}r_{\text{ij}}}. \quad (2)$$

The variable, k^{bond} represents the axial bond stiffness; r_{i} is the stretched bond length; r_{oi} is the equilibrium bond length; k^{angle} is the torsional bond stiffness; θ_{i} is the bent bond angle; θ_{oi} is the equilibrium bond angle; k^{dihedral} is the torsional bond stiffness; n is the periodicity of the crystal structure or the number of instances of a plane of a given orientation; ϕ is the angle between adjacent planes; γ is the equilibrium value of ϕ defined on a per-atom basis; ''O'' (omicron) is the angle between the first three atoms in a tetrahedral structure where there is no crystal periodicity, i.e., $(n = 0)$, ε_{ij} the maximum depth of the energy potential well for atomic separation; σ_{ij} is the distance between atom i and atom j at which the energy is zero; r_{ij} is the atomic separation distance; q_{i} and q_{j} are the charges of the respective atoms; ε_{o} is the permittivity of free space; and r_{ij} is the distance separating atom i and atom j.

Axial modulus

Data output from the NAMD software in the form of energy and displacement was converted to force/displacement. Energy was determined by utilizing the equations in Li and Wu (1), which govern the bonding interactions between atomic groups. These equations utilize the CHARMM parameter sets as well as atomic position at each interval of the testing procedure. As the procedure is displacement-controlled, the resulting energy was converted to axial force by dividing the resulting energy by the given axial displacement at each increment, $f = U_{\text{total}}/\Delta L$. Strain was obtained by dividing the incremental displacement by the total length of each monomer ($\varepsilon = \Delta L/L_z$). The axial lengths of the template α- and β-monomers were determined to be 5.789 nm and 6.042 nm, respectively. Note that these dimensions are greater than the value of 4 nm typically reported in the literature. This discrepancy is caused by the overlap of ~2 nm between the monomers in their lattice configuration. The axial period of the center-to-center locations of individual monomers is ~4 nm, while their overall length is closer to 6 nm. Stress was calculated by determining the force per unit cross-sectional area, $\sigma = F/A_{\text{xy}}$. For α- and β-tubulin, cross-sectional area was determined by averaging the area of three least-squares ellipses drawn about the surface in the transverse direction at the center of the structure, at 40 and 60% of the distance between bottommost and topmost of the steered and fixed atoms. The resulting in-average transverse cross-sectional areas of α and β were 25.43 nm^2 and 27.88 nm^2, respectively. This algorithm was applied to all structures to estimate the molecular cross-sectional area. All simulations were run at a constant temperature of 300 K.

Stress/strain curves for the simulated tensile tests were then produced for all simulations. The qualitative behavior of each of the simulations indicate that the individual molecules respond in a manner similar to that of macroscale material sample responds under tensile load, with the exception that slope variations associated with discrete binding events at the molecular scale are undetectable in a macroscale tensile test.

Circumferential modulus

When a microtubule is stretched, monomers interact both axially and circumferentially. While the precise response to multiaxial loading has yet to be determined, it is assumed that tubulin monomers will exhibit anisotropic behavior based on both their antisymmetric structure and their assembly modes (18). Thus, to determine the degree of anisotropy, the tensile tests described above were repeated on all structures in the circumferential direction. The axis of applied displacement we used was chosen to simulate the forces imposed by the binding with conjoining dimers within the helical structure of the microtubule.

With a total of 538 stress/strain curves produced (269 curves for axial tensile models and 269 curves for circumferential tensile models), we plotted our predicted elastic modulus values against the following physical parameters as determined by Tuszynski et al. (19): net dipole moment; net charge; volume; and surface area. Further characteristics such as number of residues, cross-sectional area, number of atoms, homology similarity, and percent distribution of each individual amino acid were also plotted as a function of the axial elastic modulus. Linear regression statistics demonstrated that, while none of these characteristics produced any observable trends, one prominent trend was an inverse correlation between axial stiffness and axial length.

Polyglycine simulations

To test the effects of simulation size on elastic modulus results, we also performed identical simulations on both linear and helical oligomeric glycine chains of lengths ranging from 10 Å to 500 Å. The first and last group of residues in the structure was deemed as fixed and steered atoms. The simulation directed a linear displacement along the axial direction of the glycine chain. These simulations were used to determine whether long-range electrostatic interactions contributed significantly to the simulation energy. Specifically, as the chains are stretched, covalent interactions dominate electrostatic interactions. Additionally, increasing the chain length of an oligomeric structure in vacuo was expected to artificially stiffen the structure as more residues are added, since additional residues added to either end may still interact with interior residues. This trend is expected to continue until a length is reached at which these boundary conditions become less prevalent.

RESULTS

Axial modulus

As seen in the stress/strain curves in Figs. 4 *b* and 5, our simulations demonstrate a failure curve reminiscent of polymerlike failure curves. There is an elastic region from 0 to 0.350 strain, followed by plastic deformation from 0.350 to 0.475 strain, and ultimately failure above 0.475 strain. These particular values are unique to the bovine β-tubulin structure. However, this overall shape was demonstrated by both the α- and β-template 1JFF monomers. In nature, a strain of 0.3 or greater is highly unlikely to ever occur. However, as microtubules have recently been used as potential components for nanomachinery (e.g., (43,44)), this may become a critical design parameter.

The axial modulus for each monomer was calculated in a manner similar to those outlined by Shah (45). For α-tubulin, the modulus was 12.51 pN/Å^2 (1.25 GPa). For β-tubulin, the modulus was 13.35 pN/Å^2 (1.34 GPa). These values agree well with other recent AFM and finite element analysis results that predict the modulus to be ~1.4 GPa (46). To evaluate whether our predicted elastic moduli agree with recently measured mechanical properties of single microtubules, we developed a beam-mechanics model wherein each monomer was given a spring constant, k, based on its predicted modulus, E, its area, A, and its length, L, via $k = EA/L$ (see Appendix). We also assigned spring constants to the α-β binding site and the β-α binding sites, giving them values 0.1, 1.0, and 10 times that of the monomer stiffness. For these values, we found persistence lengths of 0.4, 2.3, and 4.1 mm, respectively. This agrees remarkably well with the recent empirical results of Pampaloni et al. (47), who found MT persistence lengths to range between 0.2 and 5 mm for MTs ranging in length from 2 to 40 μm.

To quantify correlation between monomer geometry and elastic modulus, we plotted all moduli as a function of monomer length (Fig. 6). These data are summarized in Table 2. Our primary finding was that as monomer axial length increased, axial stiffness decreased. The regression lines for the α- and

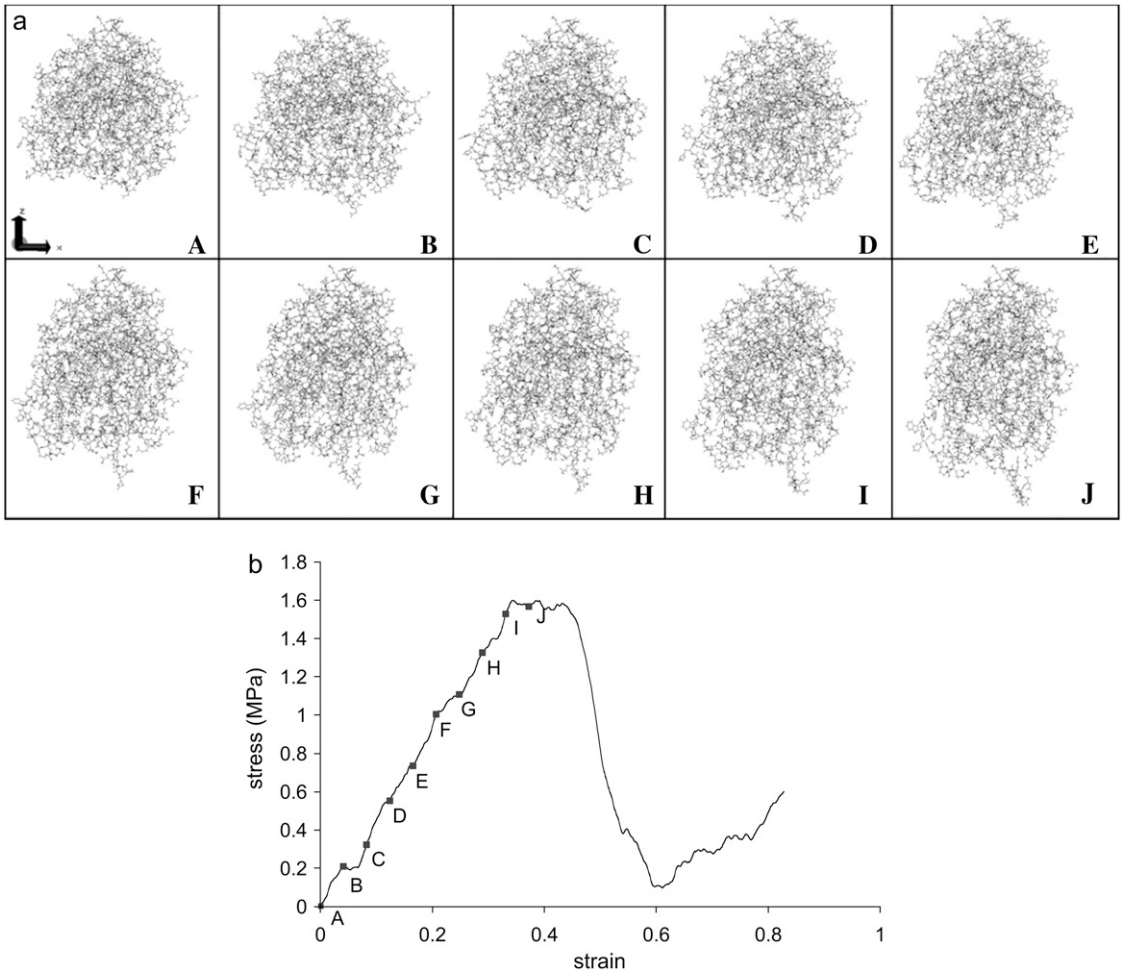

FIGURE 4 (*a*) Incrementally stretched structure of 1JFFB (σ, stress; ε, strain). (*A*) $\varepsilon = 0.00$, $\sigma = 0.00$ MPa; (*B*) $\varepsilon = 0.041$ $\sigma = 210$; (*C*) $\varepsilon = 0.083$, $\sigma = 323$; (*D*) $\varepsilon = 0.124$, $\sigma = 522$; (*E*) $\varepsilon = 0.166$, $\sigma = 735$; (*F*) $\varepsilon = 0.207$, $\sigma = 1005$; (*G*) $\varepsilon = 0.248$, $\sigma = 1107$; (*H*) $\varepsilon = 0.290$, $\sigma = 1326$; (*I*) $\varepsilon = 0.331$, $\sigma = 1528$; and (*J*) $\varepsilon = 0.372$, $\sigma = 1567$. (*b*) Stress/strain plot for IJFFB.

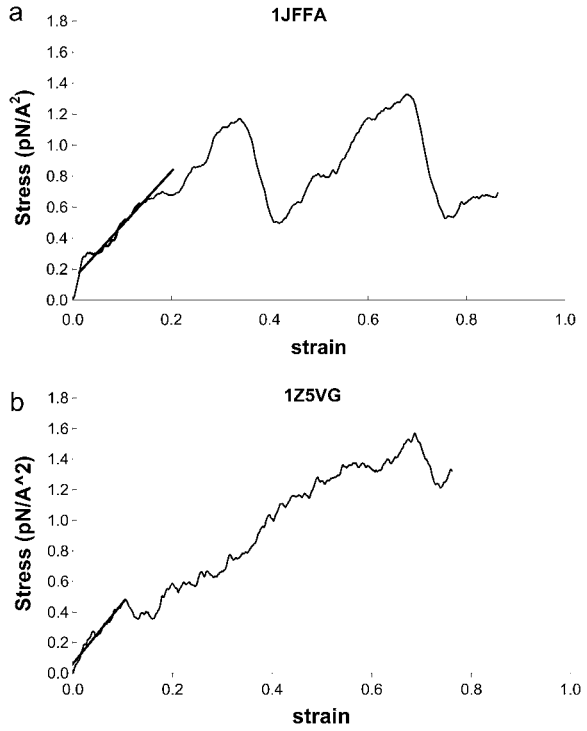

FIGURE 5 Example stress-strain curves of other tubulin monomers demonstrating multimodulus behavior. (*a*) 1JFFA; (*b*) 1Z5VG.

β-data are almost identical. For α-structures, $\sigma = -22.32\varepsilon + 2649.9$ MPa, with an R^2 of 0.8233. For β-structures, $\sigma = -24.07\varepsilon + 2861.5$ MPa with an R^2 of 0.4177. While we are reticent to make further predictions from the current data set, it could be that the high degree of similarity between these trends is a result of the tertiary interactions specific to tubulin. A similar trend was seen with the γ-tubulin simulations. However, since the range of lengths of the γ-monomers was significantly diminutive compared with those of α and β, only an insignificant correlation was found ($R^2 = 0.0489$).

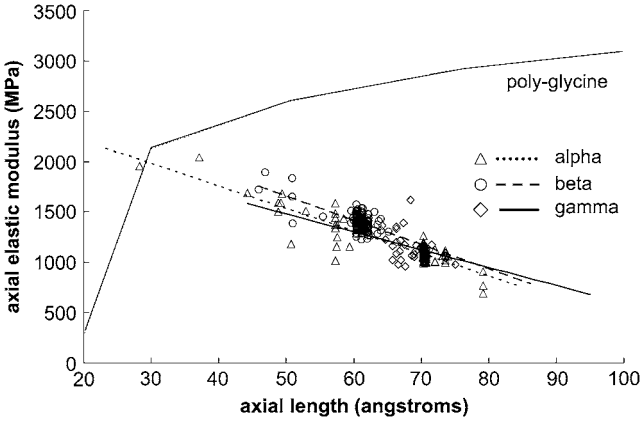

FIGURE 6 Axial elastic modulus as a function of monomer length for α-tubulin (*triangles*), β-tubulin (*circles*), and γ-tubulin (*diamonds*). Top trace is that of polyglycine.

Typical bond energies are -9.1×10^{-21} to -2.4×10^{-20} J laterally and -2.8×10^{-20} to -3.9×10^{-20} J longitudinally (48). The typical work-to-failure of most our model systems were -5.1×10^{-18} J for β and -3.0×10^{-18} J for α. This is consistent with the observation that microtubule failure occurs between, rather than within, monomers.

Circumferential modulus

Elastic moduli in the circumferential direction were approximately one-third of those in the axial direction. To our knowledge, this is the first report of tubulin anisotropy at the tertiary level. We found an average circumferential elastic modulus of 935.6 MPa for α and 658.4 MPa for β across all structures. The circumferential elastic moduli of the α, β, and γ yielded no discernible trends as a function of axial length, circumferential length, cross-sectional area, volume, net charge, net dipole moment, residue fraction, number of atoms or number of residues—i.e., regression statistics demonstrated no significant correlation between the properties predicted by Tuszynski and monomer length. The results for circumferential modulus as a function of circumferential length are shown in Fig. 7 and summarized in Table 3.

Since we performed simulated stretching on the flat rather than the curved form of tubulin, the question remains open as to whether our results would be similar if the curved form found in MTs were to have been used. Paramount in this consideration is whether the superposition principle of mechanics (49) may be applied to MD. The superposition principle, as it applies to beam equations, states that the stress or strain state resulting from the three primary modes of loading (tension/compression, bending, or torsion) may be calculated separately and summed to find the overall state of the system. For example, if a beam is loaded in pure tension and subsequently in bending, the resulting stress state is the sum of the two. To our knowledge, such an investigation has not been undertaken in the MD literature, but deserves investigation. For the current work, the possibility exists that either or both of the axial results and circumferential results would be affected by simulating the curved versus the flat state. For example, as recently demonstrated by Krebs et al. (24), axially, the splayed state of a depolymerizing microtubule represents an intermediately stable form with a radius of curvature of ~100–200 nm about the θ-axis. In the circumferential direction, both the sheet conformation and the cylindrical conformation represent stable forms depending on the phosphorylation state of β-tubulin.

Polyglycine simulations

The polyglycine control simulations resulted in an inverse trend: longer structures were stiffer than shorter structures and approached an asymptote near a length of 75 Å. This effect is attributable to long-range interactions among individual atoms in the simulation, i.e., central atoms are affected by a greater number of boundary atoms, but as the fraction of

TABLE 2 Tabular data of all axial moduli

Alpha				Beta						Gamma	
1JFFA	1251	TBA1_SCHPO	1017	1JFFB	1335	TBB_TETTH	1325	TBB2_HOMAM	1310	1Z5VG	1491
TBA_AVESA	1051	TBA1_STYLE	1073	TBB_ACHKL	1405	TBB_THAWE	1336	TBB2_HUMAN	1453	TBG_ANEPH	1117
TBA_BOMMO	1080	TBA1_VOLCA	1068	TBB_ACRCO	1473	TBB_TOXGO	1389	TBB2_LUPAL	1259	TBG_CAEEL	1618
TBA_CANAL	1583	TBA1_YEAST	1336	TBB_AJECA	1498	TBB_TRYBR	1376	TBB2_MAIZE	1313	TBG_CANAL	1361
TBA_CHLVU	1115	TBA2_ARATH	1077	TBB_ASPFL	1398	TBB_TRYCR	1396	TBB2_ORYSA	1355	TBG_CHLRE	977
TBA_DICDI	1370	TBA2_CAEEL	1153	TBB_ASPPA	1410	TBB_VENIN	1444	TBB2_PEA	1342	TBG_EMENI	1170
TBA_EUGGR	1046	TBA2_CHICK	1060	TBB_BABBO	1403	TBB_YEAST	1462	TBB2_PHYPO	1320	TBG_ENTHI	1176
TBA_EUPOC	1015	TBA2_CHLRE	1054	TBB_BOMMO	1403	TBB1_ANEPH	1476	TBB2_PORPU	1317	TBG_EUPAE	1163
TBA_EUPVA	1259	TBA2_DROME	1000	TBB_BOTCI	1338	TBB1_ARATH	1377	TBB2_SOLTU	1280	TBG_NEUCR	1110
TBA_HAECO	1006	TBA2_ELEIN	1110	TBB_CANAL	1385	TBB1_BRUPA	1339	TBB2_SOYBN	1411	TBG_PHYPA	1351
TBA_MYCGR	768	TBA2_EMENI	1481	TBB_CEPAC	1310	TBB1_CHICK	1379	TBB2_TRIVI	1474	TBG_RETFI	1388
TBA_NOTVI	1125	TBA2_HOMAM	1087	TBB_CHLIN	1459	TBB1_CHOCR	1342	TBB2_WHEAT	1376	TBG_SCHJP	1054
TBA_OCTDO	1043	TBA2_HORVU	996	TBB_CHLRE	1444	TBB1_COLGR	1377	TBB2_XENLA	1413	TBG_SCHPO	1064
TBA_OCTVU	1178	TBA2_HUMAN	1111	TBB_CICAR	1424	TBB1_CYAPA	1364	TBB3_CHICK	1441	TBG_USTVI	1150
TBA_ONCKE	1001	TBA2_MAIZE	1021	TBB_DICDI	1405	TBB1_ELEIN	1356	TBB3_DROME	1282	TBG_YEAST	1117
TBA_OXYGR	1113	TBA2_MOUSE	1092	TBB_EIMTE	1222	TBB1_EMENI	1385	TBB3_ELEIN	1383	TBG1_HUMAN	958
TBA_PIG	1071	TBA2_NEUCR	690	TBB_EPITY	1455	TBB1_GADMO	1249	TBB3_MAIZE	1370	TBG1_MAIZE	1333
TBA_PLAFK	991	TBA2_PATVU	1043	TBB_ERYGR	1392	TBB1_GEOCN	1457	TBB3_ORYSA	1309	TBG1_MOUSE	1172
TBA_PLAYO	1022	TBA2_PELFA	1094	TBB_EUGGR	1511	TBB1_HOMAM	1428	TBB3_PEA	1267	TBG2_ARATH	1084
TBA_PRUDU	1123	TBA2_SCHPO	1128	TBB_EUPCR	1282	TBB1_HUMAN	1350	TBB3_PORPU	1382	TBB3_SOYBN	1386
TBA_SORMA	693	TBA2_STYLE	1102	TBB_EUPFO	1299	TBB1_LUPAL	1433	TBB3_SOYBN	1386	TBG2_EUPCR	1021
TBA_TETPY	1003	TBA3_ARATH	1154	TBB_EUPOC	1319	TBB1_MAIZE	1472	TBB3_WHEAT	1332	TBG2_EUPOC	1021
TBA_TETTH	1043	TBA3_DROME	1104	TBB_GIALA	1533	TBB1_MANSE	1414	TBB4_ARATH	1357	TBG2_HUMAN	1217
TBA_TORMA	1132	TBA3_ELEIN	1062	TBB_GIBFU	1329	TBB1_NOTCO	1477	TBB4_CAEEL	1497	TBG2_MAIZE	1199
TBA_TOXGO	1143	TBA3_HOMAM	1090	TBB_HALDI	1450	TBB1_ORYSA	1336	TBB4_CHICK	1450	TBG2_MOUSE	1108
TBA_TRYBR	1136	TBA3_HORVU	1068	TBB_HORVU	1352	TBB1_PARTE	1369	TBB4_ELEIN	1313	TBG2_ORYSA	976
TBA_TRYCR	1010	TBA3_MAIZE	1199	TBB_MYCPJ	1575	TBB1_PEA	1405	TBB4_HUMAN	1387	TBG3_MAIZE	1222
TBA_WHEAT	1097	TBA3_MOUSE	1035	TBB_NAEGR	1443	TBB1_PHYPO	1404	TBB4_MAIZE	1233		
TBA_XENLA	1036	TBA3_YEAST	1441	TBB_NEUCR	1381	TBB1_PORPU	1487	TBB4_PORPU	1440		
TBA1_ANEPH	1000	TBA4_DROME	1152	TBB_OCTDO	1406	TBB1_RAT	1352	TBB4_WHEAT	1299		
TBA1_ARATH	1159	TBA5_CHICK	1162	TBB_ONCGI	1264	TBB1_SOLTU	1367	TBB4_XENLA	1402		
TBA1_CHICK	1249	TBA5_MAIZE	1143	TBB_PARLI	1449	TBB1_SOYBN	1462	TBB5_ARATH	1334		
TBA1_CHLRE	1101	TBA6_ARATH	1037	TBB_PENDI	1377	TBB1_TRIVI	1347	TBB5_CHICK	1485		
TBA1_DROME	1108	TBA6_HUMAN	1033	TBB_PESMI	1290	TBB1_VOLCA	1488	TBB5_ECTVR	1489		
TBA1_ELEIN	1115	TBA6_MAIZE	1089	TBB_PHANO	1360	TBB1_WHEAT	1405	TBB5_MAIZE	1346		
TBA1_EMENI	904	TBA6_MOUSE	1051	TBB_PHYCI	1505	TBB2_ANEPH	1348	TBB5_WHEAT	1377		
TBA1_ENTHI	1436	TBA8_HUMAN	997	TBB_PIG	1315	TBB2_CAEEL	1423	TBB6_CHICK	1415		
TBA1_HORVU	1065	TBAA_SCHCO	1068	TBB_PLAFK	1407	TBB2_CHICK	1276	TBB6_ECTVR	1381		
TBA1_HUMAN	1130			TBB_PLESA	1416	TBB2_COLGL	1322	TBB6_MAIZE	1292		
TBA1_MAIZE	1073			TBB_PNECA	1400	TBB2_COLGR	1330	TBB7_ARATH	1432		
TBA1_MOUSE	1080			TBB_POLAG	1383	TBB2_DAUCA	1426	TBB7_CHICK	1379		
TBA1_NEUCR	1367			TBB_PSEAM	1511	TBB2_DROER	1365	TBB7_MAIZE	1389		
TBA1_ORYSA	1179			TBB_RHYSE	1358	TBB2_DROME	1355	TBB8_ARATH	1293		
TBA1_PARLI	1116			TBB_SCHCO	1441	TBB2_ELEIN	1372	TBB8_MAIZE	1397		
TBA1_PEA	1126			TBB_SCHPO	1472	TBB2_EMENI	1468	TBB9_ARATH	1333		
TBA1_PELFA	1060			TBB_STYLE	1435	TBB2_ERYPI	1437				
TBA1_PNECA	1005	Avg. 1098 ± 136		TBB_TETPY	1537	TBB2_GEOCN	1524	Avg. 1388 ± 68		Avg. 1162 ± 151	

boundary atoms diminishes, so does this effect. This correlation stood in direct contrast to the inverse correlation between axial stiffness and axial length, thus bolstering the validity of our approach.

DISCUSSION

We have used a molecular mechanics approach to perform tensile tests on individual tubulin monomers and determined values for elastic moduli for all currently known complete sequences. The results obtained from the simulations for each species were tabulated for cross-species comparisons. Sequences were chosen by Keeling and Doolittle, who demonstrated the divergent evolution of tubulin structures (50). Carpenter et al. (51) built upon Keeling and Doolittle's homology models, calculating structural and physical properties for >300 sequences, noting that a large fraction of these monomeric structures were incomplete. We have found that the axial modulus of elasticity decreases as a function of monomer length, whereas the circumferential modulus showed no such trend.

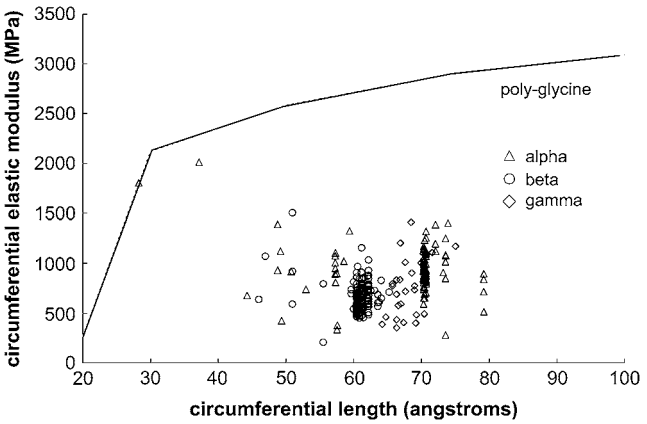

FIGURE 7 Circumferential elastic modulus as a function of monomer length for α-tubulin (*triangles*), β-tubulin (*circles*), and (*c*) γ-tubulin (*diamonds*). Top trace is that of polyglycine.

Our approach of mapping primary sequences to a known three-dimensional structure was necessary since the problem of de novo prediction of three-dimensional structure from a one-dimensional sequence is an exceedingly difficult problem and frequently yields nonunique solutions (29). We view this approach as a preliminary step toward quantifying tubulin's material response to axial loading and predicting tubulin's mechanical behavior in other loading modes such as bending, tension, and torsion. For example, predicting how a microtubule will bend or buckle under load may help explain specific functions of microtubules during mitosis or of their interactions with surrounding membranes. While the anisotropy of whole microtubules has been discussed elsewhere (18,52), to our knowledge, this relationship has not been simulated or demonstrated for any globular protein structure.

One potential limitation of our approach is that since we used bovine tubulin as our template structure, the possibility exists that our predicted structures likely had conformations similar to that of the template, and that this may have resulted in our predicted structures being confined to a local energy minimum rather than the global energy minimum. Restated, the method we chose for energy minimization is likely to have found the energy minimum closest to that of the bovine tubulin. The possibility exists that we did not find the global minimum. Other methods, such as the conformational space annealing genetic algorithms, have been shown to more efficiently and effectively find global minimums (53,54). However, what has not yet been determined is whether the predicted global minimum represents the in vivo state of the protein. Thus, finding a global minimum, while certainly providing an unequivocal standard for protein structure prediction, to our knowledge, has yet to be systematically compared to in vivo protein structure.

We also found reasonable agreement between the predicted moduli of the monomers simulated and the global behavior of individual MTs (47). One limitation of our beam analysis is that we did not include a separate stiffness for the axial monomer-monomer bonds versus the dimer-dimer bonds. Since the native form of tubulin in the cell is dimeric rather than monomeric, it is likely that the monomer-monomer bond is stiffer than the dimer-dimer bond. However, in our order-of-magnitude approximation (Figs. 8 and 9), varying this stiffness from 0.1 to 10 times that of the predicted stiffness of individual monomers resulted in persistence length predictions all within the recent experimental results of Pampaloni et al. (47). Additionally, since the binding stiffness at the seam of the microtubule may have an energy different from that between the other filaments, this may have an effect on the MT-scale mechanical behavior. This is likely to manifest itself if shear interactions are accounted for. In our first-order analysis, we only considered axial interactions. An analysis that does include shear interactions (e.g., (47)) may benefit by assigning a separate shear modulus to this portion of the structure.

Unfortunately, no other empirical three-dimensional atomistic models of tubulin species exist. Previous studies, such as Tuszynski et al. (19), used software such as MODELLER to create the homologous structures to the template protein. However, because of the large number of structures under investigation in our study, we decided to use protocol SWISS-MODEL because of its known speed and accuracy. An additional limitation of our study is that most of the high-resolution structures have been determined from crystalline preparations and are likely different from the native tubular form. However, since it is likely that tubulin oscillates about some minimal energy tertiary conformation in vivo, it seems reasonable to use the models generated by SWISS-MODEL (55) as approximations to demonstrate trends in stiffness behavior.

Presumably, as tubulin evolves, it performs a balancing act by maintaining a sequence that allows it to not only attain a structure that is mechanically the most efficient for sustaining compressive loads (i.e., a hollow cylinder) but also allows for rapid assembly and disassembly. Through evolution, the sequences within each species it serves change in a combination of ways that nature deems as either beneficial or detrimental, as it meets, or fails to meet, demands from external pressures (e.g., (19)). Through an intergenomic mechanical analysis such as ours, a demonstration of how evolution has affected the structure and strength of this protein may become possible. For example, by further analyzing the positions within the phylogenic tree of tubulin sequences and the tubulin's mechanical characteristics, a clearer picture emerges of what specific key mutations may have occurred to meet new demands. These techniques may also enable engineering of the tubulin sequence and thus the monomer structure to modify microtubule polymerization and mechanical loading characteristics.

It is important to note that the accuracy of the results depend greatly on the original PDB structure. With this in mind, these simulations do offer an approximate model to in situ behavior while offering insight into mechanical properties as well as overall trends. For example, we anticipate that, once

TABLE 3 Tabular data of all circumferential moduli

Alpha				Beta						Gamma	
1JFFA	378	TBA1_STYLE	1038	1JFFB	460	TBB_THAWE	583	TBB2_LUPAL	741	1N5VG	401
TBA_AVESA	1126	TBA1_VOLCA	961	TBB_ACHKL	503	TBB_TOXGO	538	TBB2_MAIZE	506	TBG_ANEPH	493
TBA_BOMMO	1111	TBA1_YEAST	1075	TBB_ACRCO	524	TBB_TRYBR	628	TBB2_ORYSA	767	TBG_CAEEL	1412
TBA_CANAL	1007	TBA2_ARATH	921	TBB_AJECA	729	TBB_TRYCR	554	TBB2_PEA	778	TBG_CANAL	390
TBA_CHLVU	591	TBA2_CAEEL	1326	TBB_ASPFL	574	TBB_VENIN	602	TBB2_PHYPO	908	TBG_CHLRE	1172
TBA_DICDI	380	TBA2_CHICK	1403	TBB_ASPPA	553	TBB_YEAST	680	TBB2_PORPU	908	TBG_EMENI	484
TBA_EUGGR	920	TBA2_CHLRE	1144	TBB_BABBO	799	TBB1_ANEPH	847	TBB2_SOLTU	685	TBG_ENTHI	1109
TBA_EUPOC	755	TBA2_DROME	1122	TBB_BOMMO	456	TBB1_ARATH	645	TBB2_SOYBN	927	TBG_EUPAE	773
TBA_EUPVA	829	TBA2_ELEIN	882	TBB_BOTCI	695	TBB1_BRUPA	572	TBB2_TRIVI	613	TBG_NEUCR	401
TBA_HAECO	817	TBA2_EMENI	809	TBB_CANAL	682	TBB1_CHICK	697	TBB2_WHEAT	777	TBG_PHYPA	354
TBA_MYCGR	715	TBA2_HOMAM	931	TBB_CEPAC	557	TBB1_CHOCR	748	TBB2_XENLA	564	TBG_RETFI	405
TBA_NOTVI	831	TBA2_HORVU	281	TBB_CHLIN	633	TBB1_COLGR	742	TBB3_CHICK	504	TBG_SCHJP	775
TBA_OCTDO	936	TBA2_HUMAN	928	TBB_CHLRE	717	TBB1_CYAPA	602	TBB3_DROME	606	TBG_SCHPO	903
TBA_OCTVU	919	TBA2_MAIZE	1014	TBB_CICAR	657	TBB1_ELEIN	619	TBB3_ELEIN	752	TBG_USTVI	1005
TBA_ONCKE	872	TBA2_MOUSE	1100	TBB_DICDI	612	TBB1_EMENI	652	TBB3_MAIZE	659	TBG_YEAST	1040
TBA_OXYGR	988	TBA2_NEUCR	514	TBB_EIMTE	617	TBB1_GADMO	497	TBB3_ORYSA	608	TBG1_HUMAN	717
TBA_PIG	812	TBA2_PATVU	995	TBB_EPITY	704	TBB1_GEOCN	968	TBB3_PEA	791	TBG1_MAIZE	689
TBA_PLAFK	851	TBA2_PELFA	1114	TBB_ERYGR	591	TBB1_HOMAM	828	TBB3_PORPU	671	TBG1_MOUSE	1010
TBA_PLAYO	897	TBA2_SCHPO	1197	TBB_EUGGR	694	TBB1_HUMAN	684	TBB3_SOYBN	476	TBG2_ARATH	834
TBA_PRUDU	928	TBA2_STYLE	1235	TBB_EUPCR	786	TBB1_LUPAL	730	TBB3_WHEAT	635	TBG2_DROME	733
TBA_SORMA	840	TBA3_ARATH	652	TBB_EUPFO	712	TBB1_MAIZE	643	TBB4_ARATH	518	TBG2_EUPCR	594
TBA_TETPY	654	TBA3_DROME	792	TBB_EUPOC	686	TBB1_MANSE	686	TBB4_CAEEL	546	TBG2_EUPOC	793
TBA_TETTH	898	TBA3_ELEIN	1052	TBB_GIALA	622	TBB1_NOTCO	790	TBB4_CHICK	476	TBG2_HUMAN	1204
TBA_TORMA	838	TBA3_HOMAM	1105	TBB_GIBFU	671	TBB1_ORYSA	785	TBB4_ELEIN	679	TBG2_MAIZE	435
TBA_TOXGO	692	TBA3_HORVU	1085	TBB_HALDI	209	TBB1_PARTE	527	TBB4_HUMAN	735	TBG2_MOUSE	835
TBA_TRYBR	738	TBA3_MAIZE	962	TBB_HORVU	590	TBB1_PEA	872	TBB4_MAIZE	656	TBG2_ORYSA	579
TBA_TRYCR	943	TBA3_MOUSE	1099	TBB_MYCPJ	464	TBB1_PHYPO	594	TBB4_PORPU	849	TBG3_MAIZE	461
TBA_WHEAT	1075	TBA3_YEAST	1107	TBB_NAEGR	913	TBB1_PORPU	573	TBB4_WHEAT	620		
TBA_XENLA	897	TBA4_DROME	900	TBB_NEUCR	508	TBB1_RAT	486	TBB4_XENLA	603		
TBA1_ANEPH	988	TBA5_CHICK	707	TBB_OCTDO	452	TBB1_SOLTU	569	TBB5_ARATH	713		
TBA1_ARATH	765	TBA5_MAIZE	844	TBB_ONCGI	726	TBB1_SOYBN	665	TBB5_CHICK	675		
TBA1_CHICK	336	TBA6_ARATH	1026	TBB_PARLI	722	TBB1_TRIVI	649	TBB5_ECTVR	743		
TBA1_CHLRE	1012	TBA6_HUMAN	1072	TBB_PENDI	561	TBB1_VOLCA	655	TBB5_MAIZE	879		
TBA1_DROME	1322	TBA6_MAIZE	964	TBB_PESMI	658	TBB1_WHEAT	930	TBB5_WHEAT	622		
TBA1_ELEIN	1252	TBA6_MOUSE	921	TBB_PHANO	565	TBB2_ANEPH	859	TBB6_ARATH	507		
TBA1_EMENI	895	TBA8_HUMAN	1120	TBB_PHYCI	688	TBB2_ARATH	567	TBB6_CHICK	846		
TBA1_ENTHI	1021	TBA8_MOUSE	872	TBB_PIG	517	TBB2_CAEEL	559	TBB6_ECTVR	568		
TBA1_HOMAM	1121	TBAA_SCHCO	908	TBB_PLAFA	715	TBB2_CHICK	690	TBB6_MAIZE	594		
TBA1_HORVU	806			TBB_PLAFK	761	TBB2_COLGL	537	TBB7_ARATH	598		
TBA1_HUMAN	841			TBB_PLESA	814	TBB2_COLGR	566	TBB7_CHICK	643		
TBA1_MAIZE	847			TBB_PNECA	602	TBB2_DAUCA	774	TBB7_MAIZE	746		
TBA1_MOUSE	1258			TBB_POLAG	1155	TBB2_DROER	522	TBB8_ARATH	1034		
TBA1_NEUCR	893			TBB_PSEAM	752	TBB2_DROME	470	TBB8_MAIZE	722		
TBA1_ORYSA	872			TBB_RHYSE	494	TBB2_ELEIN	484	TBB9_ARATH	551		
TBA1_PARLI	1094			TBB_SCHCO	543	TBB2_EMENI	684				
TBA1_PEA	1171			TBB_SCHPO	488	TBB2_ERYPI	581				
TBA1_PELFA	1148			TBB_STYLE	718	TBB2_GEOCN	685				
TBA1_PNECA	1389			TBB_TETPY	776	TBB2_HOMAM	649				
TBA1_SCHPO	950	Avg. 936 ± 216		TBB_TETTH	551	TBB2_HUMAN	860	Avg. 658 ± 134		Avg. 741 ± 293	

more-complete data is reported on the complete sequences of all tubulin-expressing organisms, mechanical characteristics may help explain why a microtubule primarily used for mitosis in one organism, may have different mechanical properties than one used primarily for locomotion in another. We hope that, eventually, an approach such as ours, augmented by more advanced knowledge of additional structures as well as the inclusion of explicit water and a more effective energy minimization technique such as conformational space annealing, may begin to elucidate how tubulin's ancestor, FtsZ (56), evolved through various species to obtain its present form. We also hope that an analysis such as ours may be used to engineer novel tubulin structures for advanced nanotechnological devices (e.g., (43,57)). We are optimistic that this intergenomic approach may open the door to bulk modeling of multiple protein systems and homologs, across other structural proteins such as collagen, or other organellar structures or DNA-binding proteins, etc.

A similar scale-dependent modulus trend is also seen in the fibrous composites material literature, where larger speci-

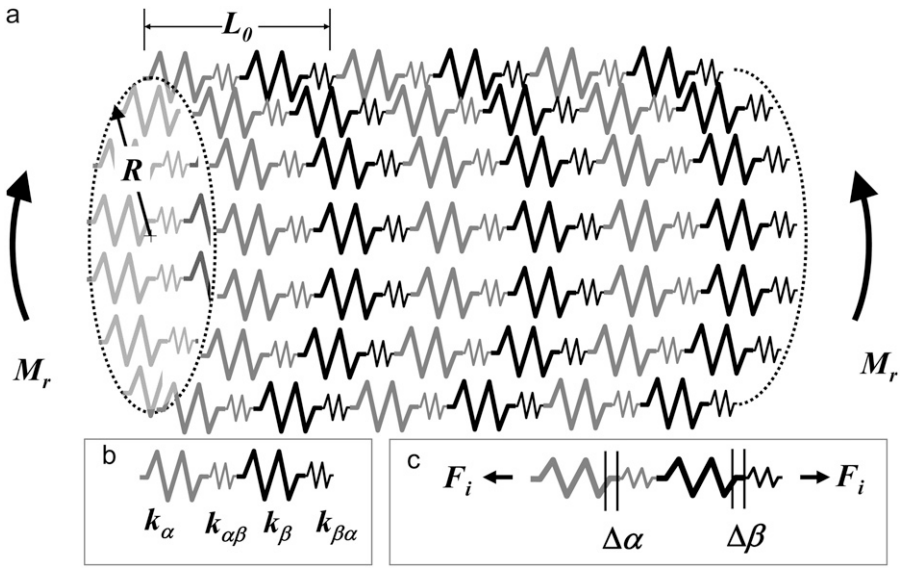

FIGURE 8 (*a*) Discrete spring model of a microtubule. M_r represents a bending moment on the microtubule. (*b*) Spring constants: k_α represents the stiffness of α-subunit, k_β is the stiffness of β-subunit, $k_{\alpha\beta}$ is the binding between α- and β-subunits, and $k_{\beta\alpha}$ is the binding between β- and α-subunits. (*c*) Forces: F_i on the i^{th} filament within the microtubule resulting from the externally applied moment causes deformations (Δ_α and Δ_β for the subunits, and $\Delta_{\alpha\beta}$ and $\Delta_{\beta\alpha}$ for the binding regions).

mens typically are weaker than smaller ones (58). This may be explained through a weakest-link analogy, whereby the more molecular bonds that are added to a structure, the more likely it becomes that a weaker bond will be added. In this work, this statistical explanation may also explain why a more compliant structure is created as additional binding sites are added. Of particular interest may be the investigation of evolutionary trends that drove tubulin to its current state as it evolved to support its myriad of mechanical roles (59,60).

Future work will include using values obtained for the elastic moduli and incorporating them into a finite element model to perform bending and buckling tests (e.g., (61)). We will assume the microtubule to be a fully stable polymerized chain. We will use the commonly accepted 13:3 lattice structure; 13 dimers with a helical pitch of 3 per complete revolution; and assemble the dimers assuming the central axis of the microtubule to be straight (62). The radius of the tube will be set to 11.2 nm (63). While the data shown in this work are for tension only, we realize that compression and torsion are also important loading modes and will be modeled in future simulations. As the mechanical properties of the different types of microtubules are determined, additional microtubules will be incorporated into the simulation. In addition, these simulations were performed in vacuo. In vivo fluid interactions may have a small but significant impact on results (e.g. (64,65)). Dimer-dimer interactions are also an important consideration (shear, multiaxial loading, etc.). Future work will include simulation of dimer structures, and ultimately the superquaternary structure of microtubules themselves.

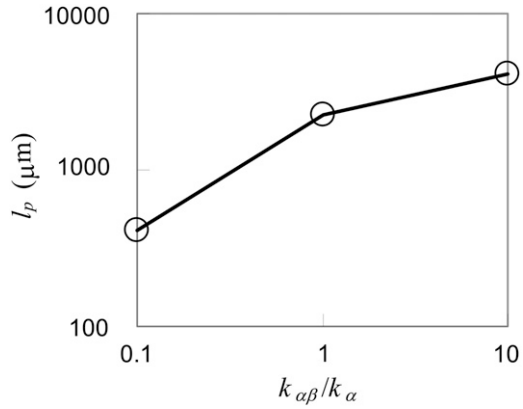

FIGURE 9 Microtubule persistence length as predicted by the ratio between the stiffness of the α-β bonds, $k_{\alpha\beta}$, and the stiffness of the α monomers, k_α. Note that since this is an order-of-magnitude analysis, we have assumed $k_{\beta\alpha}/k_\beta \cong k_{\alpha\beta}/k_\alpha$. For this simulation, we have used the calculated moduli, $E_{\mathrm{TBA\_PIG}} = 1100$ MPa, $E_{\mathrm{TBB\_PIG}} = 1300$ MPa; their predicted areas, $A_{\mathrm{TBA\_PIG}} = 25\ \mathrm{nm}^2$, $A_{\mathrm{TBB\_PIG}} = 28\ \mathrm{nm}^2$; and their predicted lengths, $L_{\mathrm{TBA\_PIG}} = 6.0$ nm, $L_{\mathrm{TBB\_PIG}} = 6.0$ nm.

APPENDIX: RELATION OF MONOMER MODULUS E_{MONO} TO MICROTUBULE MODULUS E_{MT}

Typically in composite or multiscale structures, the smaller subunits tend to be stronger and stiffer than the macroscale structure (e.g., (66)). If the predicted moduli determined by our method are to inform the tubulin-scale behavior, a multiscale approach is warranted. Beginning with the length-dependent persistence length measurements recently completed by Pampaloni et al. (47), we may make an estimate of the axial elastic modulus (Young's modulus) of a microtubule and compare it to our results. The persistence length, l_p of a molecule is defined as

$$l_\mathrm{p} = \frac{EI}{k_\mathrm{B}T}, \tag{3}$$

where E is Young's modulus of elasticity, I is the second moment of inertia, k_B is Boltzmann's constant, and T is temperature in Kelvins. An intuitive way to interpret this relationship is that l_p represents the ratio between the order-preserving EI of the numerator and the disorder-maintaining $k_\mathrm{B}T$ of the denominator. The numerator has dimensions of energy × length, while the denominator has dimensions of energy, resulting in a characteristic length that predicts how closely correlated the position of one end of a molecule (or supermolecular structure in the case of a microtubule) is with the other end. The persistence length of individual microtubules has been reported to be

5 mm for microtubules with contour lengths of 40 μm, and close to 100 nm for microtubules with contour lengths <3 μm. Solving Eq. 3 for E and using $D_0 = 25$ nm, $D_i = 10$ nm, $k_B = 1.38 \times 10^{-23}$, $T = 310$ K, and $l_p = 100$ nm to 5 mm, results in a predicted E_{MT} of 22.9 kPa to 1.14 MPa, or 3–5 orders-of-magnitude less than the E_{mono} found in our study. Thus it is likely that the binding both between and within dimers govern the microtubule's behavior. A discrete model that models spring constants of individual monomers and the spring constants of their binding follows.

The beam-bending moment equation is

$$M_r = EI\kappa, \tag{4}$$

where M_r is the bending moment about the radial axis, and κ is the beam curvature, with dimensions of length^{-1}. I.e., $\kappa = 1/\rho$, where ρ is the radius of curvature at the center of the microtubule. Eliminating EI between Eqs. 3 and 4 results in

$$l_p = \frac{M_r}{\kappa k_B T}. \tag{5}$$

The next challenge is to relate the bending moment, M_r, acting upon the microtubule to its curvature. The moment may be taken as the sum of all of the individual forces acting within each filament as

$$l_p = \frac{\sum_{i=1}^{13} \frac{F_i \times r_i}{\kappa_i}}{k_B T}, \tag{6}$$

where r_i takes on the values of $R\sin\theta_i$, where R is the effective radius of the microtubule $\sim$10.5 nm and θ is the circumferential position of the individual filaments, i.e., $\theta = 0$, $2\pi/13$, 4p/13,. . ., $24\pi/13$. The value κ has become discretized, since each filament's curvature differs, those being in compression having a greater curvature than those in tension. The force in each filament is shared by each α-subunit and each β-subunit as well as by the α-β bond and β-α bonds. Expressing F_i as a function of total bending-displacement of each of these, $\Delta_i = \Delta_\alpha + \Delta_\beta + \Delta_{\alpha\beta} + \Delta_{\beta\alpha}$ and the spring constant of each k_α, k_β, $k_{\alpha\beta}$, and $k_{\beta\alpha}$, results in

$$l_p = \frac{\sum_{i=1}^{13} \frac{\frac{\Delta_i}{K^*} \times r_i}{\kappa_i}}{k_B T}, \tag{7}$$

where $K^* = 1/k_\alpha + 1/k_\beta + 1/k_{\alpha\beta} + 1/k_{\beta\alpha}$. Assuming a consistent curvature, κ, throughout the MT, the individual displacement, Δ_i, of each monomer reduces to $\kappa_i R L_0$, where L_0 is a dimer length, R is the average radial distance of a monomer from the center of the MT, and κ_i is the curvature of the i^{th} filament ($i = 1 \ldots 13$). The spring constants, k_α and k_β, in units of N/m, may be taken directly from the simulation data and were $\sim$5 N/m. Since the spring constants for the α-β bonds and β-α bonds are not known, we may use these as the independent variables to help determine the contribution individual monomer stiffness makes to MT stiffness. The most straightforward way to do this is through the persistence length,

$$l_p = \frac{\sum_{i=1}^{13} \frac{R^2 L_0}{K^*} |\sin\theta_i|}{k_B T}. \tag{8}$$

We thank Danna Zeiger and Kathleen Allen for support and insight. The authors declare no conflicts of interest with regard to this work.

This work was funded in part by ''Nanotechnology Meets Neuroscience'' Pennsylvania Department of Health grant No. 4100026196-240418, The Keck Foundation, and a Department of Defense Graduate Research Fellowship (to A.S.Z.).

REFERENCES

1. Li, J. Y., and C. F. Wu. 2003. Perspectives on the origin of microfilaments, microtubules, the relevant chaperonin system and cytoskeletal motors—a commentary on the spirochete origin of flagella. *Cell Res.* 13:219–227.
2. Gardner, M. K., and D. J. Odde. 2006. Modeling of chromosome motility during mitosis. *Curr. Opin. Cell Biol.* 18:639–647.
3. Nogales, E. 2001. Structural insights into microtubule function. *Annu. Rev. Biophys. Biomed.* 30:397–420.
4. Baas, P. W., C. V. Nadar, and K. A. Myers. 2006. Axonal transport of microtubules: the long and short of it. *Traffic.* 7:1–9.
5. Li, C., C. Q. Ru, and A. Mioduchowski. 2006. Torsion of the central pair microtubules in eukaryotic flagella due to bending-driven lateral buckling. *Biochem. Biophys. Res. Commun.* 351:159–164.
6. Arias-Navalon, J. A., and M. L. Cuadrado-Perez. 2003. Quantum physics and consciousness. *Rev. Neurol.* 36:400.
7. Ingber, D. E. 2003. Mechanosensation through integrins: cells act locally but think globally. *Proc. Natl. Acad. Sci. USA.* 100:1472–1474.
8. Kurachi, M., M. Hoshi, and H. Tashiro. 1995. Buckling of a single microtubule by optical trapping forces: direct measurement of microtubule rigidity. *Cell Motil. Cytoskeleton.* 30:221–228.
9. Wang, H. W., and E. Nogales. 2005. Nucleotide-dependent bending flexibility of tubulin regulates microtubule assembly. *Nature.* 435:911–915.
10. Dye, R. B., S. P. Fink, and R. C. Williams, Jr. 1993. Taxol-induced flexibility of microtubules and its reversal by MAP-2 and Tau. *J. Biol. Chem.* 268:6847–6850.
11. Elbaum, M., D. Kuchnir Fygenson, and A. Libchaber. 1996. Buckling microtubules in vesicles. *Phys. Rev. Lett.* 76:4078–4081.
12. Gittes, F., B. Mickey, J. Nettleton, and J. Howard. 1993. Flexural rigidity of microtubules and actin filaments measured from thermal fluctuations in shape. *J. Cell Biol.* 120:923–934.
13. Odde, D. J., L. Ma, A. H. Briggs, A. DeMarco, and M. W. Kirschner. 1999. Microtubule bending and breaking in living fibroblast cells. *J. Cell Sci.* 112:3283–3288.
14. Vinckier, A., P. Gervasoni, F. Zaugg, U. Ziegler, P. Lindner, P. Groscurth, A. Pluckthun, and G. Semenza. 1998. Atomic force microscopy detects changes in the interaction forces between GroEL and substrate proteins. *Biophys. J.* 74:3256–3263.
15. Kasas, S., A. Kis, B. M. Riederer, L. Forro, G. Dietler, and S. Catsicas. 2004. Mechanical properties of microtubules explored using the finite elements method. *ChemPhysChem.* 5:252–257.
16. Tuszynski, J. A., J. A. Brown, E. Crawford, E. J. Carpenter, M. L. A. Nip, J. M. Dixon, and M. V. Sataric. 2005. Molecular dynamics simulations of tubulin structure and calculations of electrostatic properties of microtubules. *Math. Comput. Model.* 41:1055–1070.
17. Kerssemakers, J. W. J., E. L. Munteanu, L. Laan, T. L. Noetzel, M. E. Janson, and M. Dogterom. 2006. Assembly dynamics of microtubules at molecular resolution. *Nature.* 442:709–712.
18. Tuszynski, J. A., T. Luchko, S. Portet, and J. M. Dixon. 2005. Anisotropic elastic properties of microtubules. *Eur. Phys. J. E. Soft Matter.* 17:29–35.
19. Tuszynski, J. A., E. J. Carpenter, J. T. Huzil, W. Malinski, T. Luchko, and R. F. Luduena. 2006. The evolution of the structure of tubulin and its potential consequences for the role and function of microtubules in cells and embryos. *Int. J. Dev. Biol.* 50:341–358.
20. Lowe, J., H. Li, K. H. Downing, and E. Nogales. 2001. Refined structure of α-β-tubulin at 3.5 Å resolution. *J. Mol. Biol.* 313:1045–1057.
21. Berman, H., K. Henrick, and H. Nakamura. 2003. Announcing the worldwide Protein Data Bank. *Nat. Struct. Biol.* 10:980.
22. Bairoch, A., R. Apweiler, C. H. Wu, W. C. Barker, B. Boeckmann, S. Ferro, E. Gasteiger, H. Huang, R. Lopez, M. Magrane, M. J. Martin, D. A. Natale, C. O'Donovan, N. Redaschi, and L. S. Yeh. 2005. The Universal Protein Resource (UniProt). *Nucleic Acids Res.* 33:D154–D159.

23. Reference deleted in proof.
24. Krebs, A., K. N. Goldie, and A. Hoenger. 2005. Structural rearrangements in tubulin following microtubule formation. *EMBO Rep.* 6:227–232.
25. Aldaz, H., L. M. Rice, T. Stearns, and D. A. Agard. 2005. Insights into microtubule nucleation from the crystal structure of human γ-tubulin. *Nature.* 435:523–527.
26. Humphrey, W., A. Dalke, and K. Schulten. 1996. VMD: visual molecular dynamics. *J. Mol. Graph.* 14:33.
27. Brooks, B. R., R. E. Bruccoleri, B. D. Olafson, D. J. States, S. Swaminathan, and M. Karplus. 1983. A program for macromolecular energy, minimization, and dynamics calculations. *J. Comput. Chem.* 4:187–217.
28. MacKarell, A. D., B. Brooks, C. L. Brooks, L. Nilsson, B. Roux, Y. Won, and M. Karplus. 1998. The energy function and its parameterization with an overview of the program. *In* The Encyclopedia of Computational Chemistry. P. V. R. e. a. Schleyer, editor. John Wiley & Sons, Chichester.
29. Schwede, T., J. Kopp, N. Guex, and M. C. Peitsch. 2003. SWISS-MODEL: an automated protein homology-modeling server. *Nucleic Acids Res.* 31:3381–3385.
30. Thompson, J. D., D. G. Higgins, and T. J. Gibson. 1994. CLUSTAL W: improving the sensitivity of progressive multiple sequence alignment through sequence weighting, position-specific gap penalties and weight matrix choice. *Nucleic Acids Res.* 22:4673–4680.
31. Consortium, C. e. S. 1998. Genome sequence of the nematode *C. elegans*: a platform for investigating biology. *Science.* 282:2012–2018.
32. Hassan, S., L. Gracia, G. Vasudevan, and P. Steinbach. 2005. Computer simulation of protein-ligand interactions: challenges and applications. *In* Methods of Molecular Biology. G. U. Nienhaus, editor. Humana Press, Totowa, NJ.
33. Reference deleted in proof.
34. Cox, B. N., and J. B. Davis. 2000. Braided composites for energy absorption under tensile loading. *J. Mater. Sci.* 35:3467–3478.
35. Phillips, J. C., R. Braun, W. Wang, J. Gumbart, E. Tajkhorshid, E. Villa, C. Chipot, R. D. Skeel, L. Kale, and K. Schulten. 2005. Scalable molecular dynamics with NAMD. *J. Comput. Chem.* 26:1781–1802.
36. Bhandarkar, M., R. Brunner, C. Chipot, A. Dalke, S. Dixit, P. Grayson, J. Gullingsrud, A. Gursoy, D. Hardy, J. Hénin, W. Humphrey, D. Hurwitz, N. Krawetz, S. Kumar, M. Nelson, J. C. Phillips, A. Shinozaki, G. Zheng, and F. Zhu. 2006. NAMD User's Guide. University of Illinois and Beckman Institute, Urbana, IL.
37. Sasoglu, F. M., A. J. Bohl, and B. E. Layton. 2007. Design and microfabrication a high-aspect-ratio tapered PDMS microbeam array for parallel nanoscale force measurement and protein printing. *J. Micromech. Microeng.* 17:623–632.
38. Odom, E. M., and D. F. Adams. 1992. Specimen size effect during tensile testing of an unreinforced polymer. *J. Mater. Sci.* 27:1767–1771.
39. Rief, M., M. Gautel, F. Oesterhelt, J. M. Fernandez, and H. E. Gaub. 1997. Reversible unfolding of individual titin immunoglobulin domains by AFM. *Science.* 276:1109–1112.
40. Ward, I. M., and J. Sweeney. 2004. An Introduction to the Mechanical Properties of Solid Polymers. Wiley, West Sussex, UK.
41. Reference deleted in proof.
42. Humphrey, W., A. Dalke, and K. Schulten. 1996. VMD: visual molecular dynamics. *J. Mol. Graph.* 14:27–38.
43. Karafyllidis, I. G., and D. C. Lagoudas. 2007. Microtubules as mechanical force sensors. *Biosystems.* 88:137–146.
44. Huang, Y. M., M. Uppalapati, W. O. Hancock, and T. N. Jackson. 2005. Microfabricated capped channels for biomolecular motor-based transport. *IEEE T. Adv. Pkg.* 28:564–570.
45. Shah, V. 1998. Handbook of Plastics Testing Technology. Wiley, New York.
46. Munson, K. M., P. G. Mulugeta, and Z. J. Donhauser. 2007. Enhanced mechanical stability of microtubules polymerized with a slowly hydrolysable nucleotide analogue. *J. Phys. Chem. B.* 111:5053–5057.
47. Pampaloni, F., G. Lattanzi, A. Jonas, T. Surrey, E. Frey, and E. L. Florin. 2006. Thermal fluctuations of grafted microtubules provide evidence of a length-dependent persistence length. *Proc. Natl. Acad. Sci. USA.* 103:10248–10253.
48. VanBuren, V., D. J. Odde, and L. Cassimeris. 2002. Estimates of lateral and longitudinal bond energies within the microtubule lattice. *Proc. Natl. Acad. Sci. USA.* 99:6035–6040.
49. Shigley, J. E., C. R. Mischke, and R. G. Budynas. 2004. Mechanical Engineering Design. McGraw-Hill, New York, NY.
50. Keeling, P. J., and W. F. Doolittle. 1996. Alpha-tubulin from early-diverging eukaryotic lineages and the evolution of the tubulin family. *Mol. Biol. Evol.* 13:1297–1305.
51. Carpenter, E. J., J. T. Huzil, R. F. Luduena, and J. A. Tuszynski. 2006. Homology modeling of tubulin: influence predictions for microtubule's biophysical properties. *Eur. Biophys. J.* 36:35–43.
52. Kis, A., S. Kasas, B. Babic, A. J. Kulik, W. Benoit, G. A. Briggs, C. Schonenberger, S. Catsicas, and L. Forro. 2002. Nanomechanics of microtubules. *Phys. Rev. Lett.* 89:248101.
53. Liwo, A., C. Czaplewski, S. Oldziej, and H. A. Scheraga. 2008. Computational techniques for efficient conformational sampling of proteins. *Curr. Opin. Struct. Biol.* 18:134–139.
54. Lee, J. S., H. A. Scheraga, and S. Rackovsky. 1997. New optimization method for conformational energy calculations on polypeptides. Conformational space annealing. *J. Comput. Chem.* 18:1222–1232.
55. Peitsch, M. C. 1996. ProMod and SWISS-MODEL: internet-based tools for automated comparative protein modeling. *Biochem. Soc. Trans.* 24:274–279.
56. Nogales, E., K. H. Downing, L. A. Amos, and J. Lowe. 1998. Tubulin and FtsZ form a distinct family of GTPases. *Nat. Struct. Biol.* 5:451–458.
57. Boal, A. K., H. Tellez, S. B. Rivera, N. E. Miller, G. D. Bachand, and B. C. Bunker. 2006. The stability and functionality of chemically crosslinked microtubules. *Small.* 2:793–803.
58. Danielson, H. E. 1945. The statistical theory of the strength of bundles of threads. I. *Proc. Roy. Soc. Lond.* 183:405–435.
59. Jekely, G., and D. Arendt. 2006. Evolution of intraflagellar transport from coated vesicles and autogenous origin of the eukaryotic cilium. *Bioessays.* 28:191–198.
60. Li, J. Y., and C. F. Wu. 2005. New symbiotic hypothesis on the origin of eukaryotic flagella. *Naturwissenschaften.* 92:305–309.
61. Allen, K. B., and B. E. Layton. 2008. Cytoskeleton—membrane interactions in neuronal growth cones: a finite element analysis study. *ASME J. Biomech. Eng.* In press.
62. Molodtsov, M. I., E. A. Ermakova, E. E. Shnol, E. L. Grishchuk, J. R. McIntosh, and F. I. Ataullakhanov. 2005. A molecular-mechanical model of the microtubule. *Biophys. J.* 88:3167–3179.
63. Li, H., D. J. DeRosier, W. V. Nicholson, E. Nogales, and K. H. Downing. 2002. Microtubule structure at 8 Å resolution. *Structure.* 10:1317–1328.
64. Trzesniak, D., and W. F. van Gunsteren. 2006. Pathway dependence of the efficiency of calculating free energy and entropy of solute-solute association in water. *Chem. Phys.* 330:410–416.
65. Leroux, V., N. Gresh, W. Q. Liu, C. Garbay, and B. Maigret. 2007. Role of water molecules for binding inhibitors in the SH2 domain of Grb2: a molecular dynamics study. *J. Mol. Struct. THEOCHEM.* 806:51–66.
66. Harlow, D. G., and S. L. Phoenix. 1978. Chain-of-bundles probability model for strength of fibrous materials. 1. Analysis and conjectures. *J. Composite Mat.* 12:195–214.
67. Pollard, T. D., and W. C. Earnshaw. 2002. Cell Biology. W. B. Saunders, New York.
68. Dobner, P. R., E. Kislauskis, B. M. Wentworth, and L. Villa-Komaroff. 1987. Alternative 5′ exons either provide or deny an initiator methi-

onine codon to the same α-tubulin coding region. *Nucleic Acids Res.* 15:199–218.

69. Strausberg, R. L., E. A. Feingold, L. H. Grouse, J. G. Derge, R. D. Klausner, F. S. Collins, L. Wagner, C. M. Shenmen, G. D. Schuler, S. F. Altschul, B. Zeeberg, K. H. Buetow, C. F. Schaefer, N. K. Bhat, R. F. Hopkins, H. Jordan, T. Moore, S. I. Max, J. Wang, F. Hsieh, L. Diatchenko, K. Marusina, A. A. Farmer, G. M. Rubin, L. Hong, M. Stapleton, M. B. Soares, M. F. Bonaldo, T. L. Casavant, T. E. Scheetz, M. J. Brownstein, T. B. Usdin, S. Toshiyuki, P. Carninci, C. Prange, S. S. Raha, N. A. Loquellano, G. J. Peters, R. D. Abramson, S. J. Mullahy, S. A. Bosak, P. J. McEwan, K. J. McKernan, J. A. Malek, P. H. Gunaratne, S. Richards, K. C. Worley, S. Hale, A. M. Garcia, L. J. Gay, S. W. Hulyk, D. K. Villalon, D. M. Muzny, E. J. Sodergren, X. Lu, R. A. Gibbs, J. Fahey, E. Helton, M. Ketteman, A. Madan, S. Rodrigues, A. Sanchez, M. Whiting, A. C. Young, Y. Shevchenko, G. G. Bouffard, R. W. Blakesley, J. W. Touchman, E. D. Green, M. C. Dickson, A. C. Rodriguez, J. Grimwood, J. Schmutz, R. M. Myers, Y. S. Butterfield, M. I. Krzywinski, U. Skalska, D. E. Smailus, A. Schnerch, J. E. Schein, S. J. Jones, and M. A. Marra. 2002. Generation and initial analysis of more than 15,000 full-length human and mouse cDNA sequences. *Proc. Natl. Acad. Sci. USA.* 99:16899–16903.

70. Rush, J., A. Moritz, K. A. Lee, A. Guo, V. L. Goss, E. J. Spek, H. Zhang, X. M. Zha, R. D. Polakiewicz, and M. J. Comb. 2005. Immunoaffinity profiling of tyrosine phosphorylation in cancer cells. *Nat. Biotechnol.* 23:94–101.

71. Kalnine N., X. Chen, A. Rolfs, A. Halleck, L. Hines, S. Eisenstein, M. Koundinya, J. Raphael, D. Moreira, T. Kelley, J. LaBaer, Y. Lin, M. Phelan, A. Farmer. Cloning of human full-length CDSs in BD Creator system donor vector. At EMBL/GenBank/DDBJ databases, May 2003.

72. Livingston R. J., M. J. Rieder, N. Rajkumar, T. K. Downing, A. N. Olson, C. P. Nguyen, H. Gildersleeve, C. M. Cassidy, E. J. Johnson, J. E. Swanson, I. McFarland, B.Yool, C. Park, and D. A Nickerson. NIEHS-SNPs, environmental genome project, NIEHS ES15478, Department of Genome Sciences, Seattle, WA. Available at http://egp.gs.washington.edu. At EMBL/GenBank/DDBJ, databases, January 2005.